

## Review

# Atlas-based ventricular shape analysis for understanding congenital heart disease<sup>☆</sup>



Genevieve Farrar<sup>a</sup>, Avan Suinesiaputra<sup>b</sup>, Kathleen Gilbert<sup>b</sup>, James C. Perry<sup>d,e</sup>, Sanjeet Hegde<sup>d,e</sup>, Alison Marsden<sup>c</sup>, Alistair A. Young<sup>b</sup>, Jeffrey H. Omens<sup>a,f</sup>, Andrew D. McCulloch<sup>a,f,\*</sup>

<sup>a</sup> Department of Bioengineering, University of California San Diego, La Jolla, CA, USA

<sup>b</sup> Department of Anatomy and Medical Imaging, University of Auckland, Auckland, New Zealand

<sup>c</sup> Department of Pediatrics, Stanford University, Stanford, CA, USA

<sup>d</sup> Division of Cardiology, Rady Children's Hospital, San Diego, CA, USA

<sup>e</sup> Department of Pediatrics, University of California San Diego, La Jolla, CA, USA

<sup>f</sup> Department of Medicine, University of California San Diego, La Jolla, CA, USA

## ARTICLE INFO

Available online 18 August 2016

## Keywords:

Cardiac  
Shape analysis  
Atlas  
Single-ventricle  
CHD

## ABSTRACT

Congenital heart disease is associated with abnormal ventricular shape that can affect wall mechanics and may be predictive of long-term adverse outcomes. Atlas-based parametric shape analysis was used to analyze ventricular geometries of eight adolescent or adult single-ventricle CHD patients with tricuspid atresia and Fontans. These patients were compared with an “atlas” of non-congenital asymptomatic volunteers, resulting in a set of Z-scores which quantify deviations from the control population distribution on a patient-by-patient basis. We examined the potential of these scores to: (1) quantify abnormalities of ventricular geometry in single ventricle physiologies relative to the normal population; (2) comprehensively quantify wall motion in CHD patients; and (3) identify possible relationships between ventricular shape and wall motion that may reflect underlying functional defects or remodeling in CHD patients. CHD ventricular geometries at end-diastole and end-systole were individually compared with statistical shape properties of an asymptomatic population from the Cardiac Atlas Project. Shape analysis-derived model properties, and myocardial wall motions between end-diastole and end-systole, were compared with physician observations of clinical functional parameters. Relationships between altered shape and altered function were evaluated *via* correlations between atlas-based shape and wall motion scores. Atlas-based shape analysis identified a diverse set of specific quantifiable abnormalities in ventricular geometry or myocardial wall motion in all subjects. Moreover, this initial cohort displayed significant relationships between specific shape abnormalities such as increased ventricular sphericity and functional defects in myocardial deformation, such as decreased long-axis wall motion. These findings suggest that atlas-based ventricular shape analysis may be a useful new tool in the management of patients with CHD who are at risk of impaired ventricular wall mechanics and chamber remodeling.

© 2016 The Authors. Published by Elsevier Ireland Ltd. This is an open access article under the CC BY-NC-ND license (<http://creativecommons.org/licenses/by-nc-nd/4.0/>).

## 1. Introduction

Cardiac malformations are the most common type of birth defect, occurring in approximately 1% of all births. Improvements in the management of congenital heart disease (CHD) have resulted in >90% of those born with CHD now surviving into early adulthood [2,3,11]. Many of these patients, particularly those with a single functional ventricle, are at risk of ventricular remodeling and dysfunction with

associated morbidity and mortality [2,17]. Heart failure (HF) is common in these patients and often develops over many years [15], but relatively little detail is known about the ventricular remodeling characteristics leading to heart failure in CHD. CHD patients commonly undergo longitudinal cardiac magnetic resonance imaging (cMRI) exams; however, standard clinical indices of mass, volume, diameter and wall thickness ignore the wealth of additional information in cMRI data regarding the more subtle or regional abnormalities in ventricular shape and wall motion that are common in these cardiac malformations.

Atlas-based shape analysis of cMRI data has shown promising results for quantifying alterations in ventricular shape in other heart diseases [13–15,17–19]. A model-based analysis of right ventricular (RV) shape identified increased eccentricity and decreased systolic function in patients with pulmonary hypertension [8]. A statistical shape analysis in

<sup>☆</sup> Supported by NIH grants 1R01HL121754 to ADM, JHO and AAY and 8P41GM103426 (the Biomedical Computation Resource) to ADM

\* Corresponding author at: Department of Medicine, University of California San Diego, La Jolla, CA, USA.

E-mail address: [amcculloch@ucsd.edu](mailto:amcculloch@ucsd.edu) (A.D. McCulloch).

repaired tetralogy of Fallot patients uncovered significant correlations of RV dilatation, outflow tract bulging, and apical dilatation with the presence of pulmonary regurgitation [9]. A study of shape analysis in myocardial infarction showed that atlas-based shape parameters classified patients from asymptomatic controls with 94% specificity and 93% sensitivity [12,14]. An MRI study using the same type of shape analysis techniques showed that young adults born pre-term had significant differences in LV mass, 3D geometry and regional wall motion that could predispose them to heart disease in later life [10].

Atlas-based cardiac shape analysis may be particularly useful for single ventricle CHD as current methods are suboptimal for assessment of remodeling and heart failure risk for these unique patients.

Eight adolescent or adult patients with tricuspid atresia and Fontan physiology were recruited for this study of shape analysis in single ventricle physiology. The three goals of this study were to: evaluate whether atlas-based shape analysis could detect and quantify relevant abnormalities in ventricular geometry in eight tricuspid atresia patients; to test a novel atlas-based assessment of ventricular function derived from shape deformations between end-diastole and end-systole; and to assess potential relationships between abnormal ventricular shape and abnormal in ventricular function in the CHD patients.

## 2. Materials and Methods

### 2.1. CHD MR Imaging Data

The datasets used in this study are part of the Cardiac Atlas Project (CAP) database\*. The CAP was established as a worldwide consortium for pooling standardized analyses of cardiac images into a database for mapping heart shape and motion [5,12,14]. Cardiac MR datasets were obtained with informed consent compatible with data sharing, and data were contributed to the CAP database with the approval of the local institutional review board. The general selection criteria for this preliminary study were: (1) a diagnosis of tricuspid atresia and hypoplastic right ventricle, (2) Fontan physiology, and (3) the patient being of adult size. Standardized procedures for the contribution, de-identification, classification, and sharing of imaging data were provided by CAP. In addition, relevant demographic and clinical data were obtained for each patient, including age, diagnoses, co-morbidities, medications, cardiac catheterization reports and echocardiography. All imaging and clinical data were de-identified in a HIPAA-compliant manner. Eight adult or teen-aged patients meeting these criteria were included in this study.

For patients 1 to 5, SSFP (Steady State Free Precession) cine images were obtained on a 1.5 T (Tesla) Philips Intera MRI scanner (Philips Medical Systems, Netherlands) using a 5-element cardiac coil using breath-holds and retrospective gating. The sequence parameters for SSFP sequence were: repetition time (TR) 2.7 ms, echo time (TE) 1.36 ms, flip angle 60 degrees, field of view (FOV) 400 mm, slice thickness 8 mm, image matrix  $192 \times 256$  and 30 heart phases.

For patients 6 to 8, images were acquired using a 1.5 T MRI scanner (Siemens Avanto; Siemens Healthcare, Erlangen, Germany) and all cines were prospectively or retrospectively gated breath-hold SSFP acquisitions. The short axis slices were acquired parallel to the tricuspid annulus plane and spanned both ventricles. Long axis slices were obtained through all valves and spanning both ventricles. The standard images parameters were as follows: slice thickness 6 mm, flip angle 60 degrees, TE 1.6 ms and TR 30 ms.

### 2.2. Clinical Data and Physician Observations

Clinical data were collected for each patient. Quantitative measurements from the images including end-diastolic volume (EDV), stroke

volume (SV), ejection fraction (EF), and left ventricular mass (LVM) were made using QMass Medis software, Leiden, The Netherlands. Volume for each image plane is calculated as the area of the endocardial tracing multiplied by the addition of the image slice thickness and inter-slice gap. End-diastolic and systolic volumes are calculated by summing all slices, which allows for calculation of stroke volume, cardiac output, and ejection fraction with standard equations [1], and are summarized in Table 1. Physician assessments of hypertrophy, dilation, and systolic dysfunction based on clinical history and reading of the MR images are summarized in Table 2 along with individual patient surgical history and additional observations. For the purposes of comparing patient data in this study, mild hypertrophy and mild dilation were defined by LV EDV and LV mass, respectively, indexed to body surface area, greater than one standard deviation greater than the mean for normal ventricles [1]. Decreased LV systolic function was defined as  $EF < 0.55$ .

### 2.3. Model Customization for CHD Data

Expert observers performed the geometric fit analysis with guide-point modeling [20] using custom software (CIM, University of Auckland, New Zealand) to create 3D ventricular anatomic models for each CHD patient based on the MR datasets. The model was interactively customized by least-squares optimization to guide points provided by the analyst, as well as computer-generated points calculated from the image using an edge detection algorithm. The model was registered to each case using fiducial landmarks defined at the mitral valve and the insertions of the right ventricular free wall into the inter-ventricular septum. Fig. 1 shows a screenshot of model customization of patient MRI data using CIM.

The LV shape model consisted of 16 elements per LV surface, for both the endocardium and the epicardium. Surface points were sampled using  $8 \times 8$  grid points per element, resulting in a total of 1682 unique 3D coordinate points for both endocardial and epicardial surfaces. A prolate spheroidal coordinate system was used to define a standardized coordinate system of the LV for each patient, registered to fiducial landmarks including the inflow valve insertion points, and apical and basal landmarks, in order to remove variations in position and orientation between cases.

### 2.4. Statistical (Population) Properties of Asymptomatic Ventricles

This study made use of previously described [13] shape models derived from cardiac MR exams of 1991 asymptomatic subjects in the CAP database. These were participants who were free from any clinical indications of cardiovascular disease at time of imaging, and were thus considered as a normal control group. In previously reported results, principal component analysis (PCA) was used to determine the dominant modes of LV shape variation in this population for both end-diastolic and end-systolic states recorded in the MR images. These statistical shape properties [13] were used for the first goal of this study: assessment of abnormalities in CHD ventricular shapes.

**Table 1**

Quantitative clinical patient data. BSA = body surface area, HR = heart rate, LV EDV = left ventricular end diastolic volume, LVEF = left ventricular ejection fraction, LV Mass = left ventricular mass. <sup>a</sup>Indicates the value is >1 standard deviation above the normal mean [1].

Patient	Age range	LV EDV (cc)	LV EDV indexed to BSA (cc/m <sup>2</sup> )	LVEF (%)	LV mass (g)	LV mass indexed to BSA (g/m <sup>2</sup> )
1	17–25	175	109 <sup>a</sup>	52	131	82 <sup>a</sup>
2	35–45	124	65	65	125	65
3	13–16	124	77	55	112	70
4	17–25	238	124 <sup>a</sup>	55	150	78
5	17–25	137	77	57	83	52
6	17–25	197	89	62	143	65
7	17–25	137	87	55	78	50
8	35–45	172	103 <sup>a</sup>	59	102	61

\* <http://www.cardiacatlas.org>.

**Table 2**  
Qualitative clinical patient data including physician observations.

Patient	LV hypertrophy	LV dilation	Systolic function	Surgeries	Other observations
1	No	Mild	Mildly diminished	Fontan, fenestration creation	Restrictive valve motion
2	No	No	Normal	Fontan (RA to MPA-LPA, SVC to RPA)	Mildly dilated ascending aorta
3	No	No	Low-normal	Damus and arch reconstruction, hemi-Fontan and Fontan	Transposed great arteries, restrictive VSD
4	No	Moderate	Low-normal	Lateral tunnel Fontan and transcatheter closure of Fontan fenestration	Mild mitral and aortic regurgitation, dilated aortic root
5	No	No	Normal	Fontan, Fontan stent	Transposed great arteries, small VSD
6	No	No	Normal	Total cavo-pulmonary connection (TCPC) Fontan	
7	No	No	Low-normal	Total cavo-pulmonary connection (TCPC) Fontan	
8	No	Borderline	Normal	Atrio-pulmonary Fontan	

For the second goal of this study, assessment of abnormalities in CHD ventricular wall motions, it was necessary to obtain statistical properties of the wall motions for the control group. Below is a brief summary of the method used to obtain the statistical shape properties for both the shapes (previously reported) and the wall motions (novel to the current study) for the asymptomatic population.

PCA has been used to extract modes of LV deformation [16], to quantify cardiac remodeling [10,21], and to identify modes of shape variation within a sub-clinical population [13]. To obtain the population statistics used here, the total input matrix size for the PCA was  $1991 \times 5046$ . That is, 1991 datasets in the asymptomatic control group, and 1682 coordinate points formatted in a row vector  $[x_1, y_1, z_1, \dots, x_M, y_M, z_M]$ , where  $M = 1682$  (and  $3 \times M = 5046$ ). We used three PCA models in this study, built from the LV shapes at (1) end-diastole ( $PCA_{ED}$ ), (2) end-systole ( $PCA_{ES}$ ), and (3) the wall motion between ED and ES frames ( $PCA_{WM}$ ). For the  $PCA_{WM}$  model, the input matrix is simply a subtraction of the surface coordinate points at ES from the corresponding coordinate points at ED. Hence, instead of variations in point locations (as in  $PCA_{ED}$  and  $PCA_{ES}$ ) the  $PCA_{WM}$  model describes variations of the displacement vectors.

The PCA procedure is described briefly as follows. Let  $\mathbf{X}$  be the input matrix and  $\bar{\mathbf{X}} = \frac{1}{N} \sum \mathbf{X}_i$  be the estimated mean shape ( $N = 1991$ ), principal components were computed using singular value decomposition (SVD) on the standardized  $(\mathbf{X} - \bar{\mathbf{X}})$  matrix. In the context of statistical shape analysis, the  $k$ -th mode of shape variation can be generated by selecting only the  $k$ -th principal component to reconstruct a shape, or

$$\mathbf{y}_k = \bar{\mathbf{X}} + \Phi \delta \mathbf{e}_k$$

where  $\Phi \in R^{3M \times 3M}$  is the principal component matrix,  $\mathbf{e}_k$  is a zero vector except the  $k$ -th component is 1, and  $\delta$  is the distance of the shape variation from the mean. A statistically plausible shape is commonly set for  $\delta$  between  $\pm 2$  times the standard deviation of the  $k$ -th eigenvalue. The first few modes characterize the dominant shape variations in the data and explain most of the shape variance in the population. These variations in shape have been related to certain types of ventricular remodeling.

Generally, the first few modes explain most of the total population variance in previous studies of ventricular shape analysis

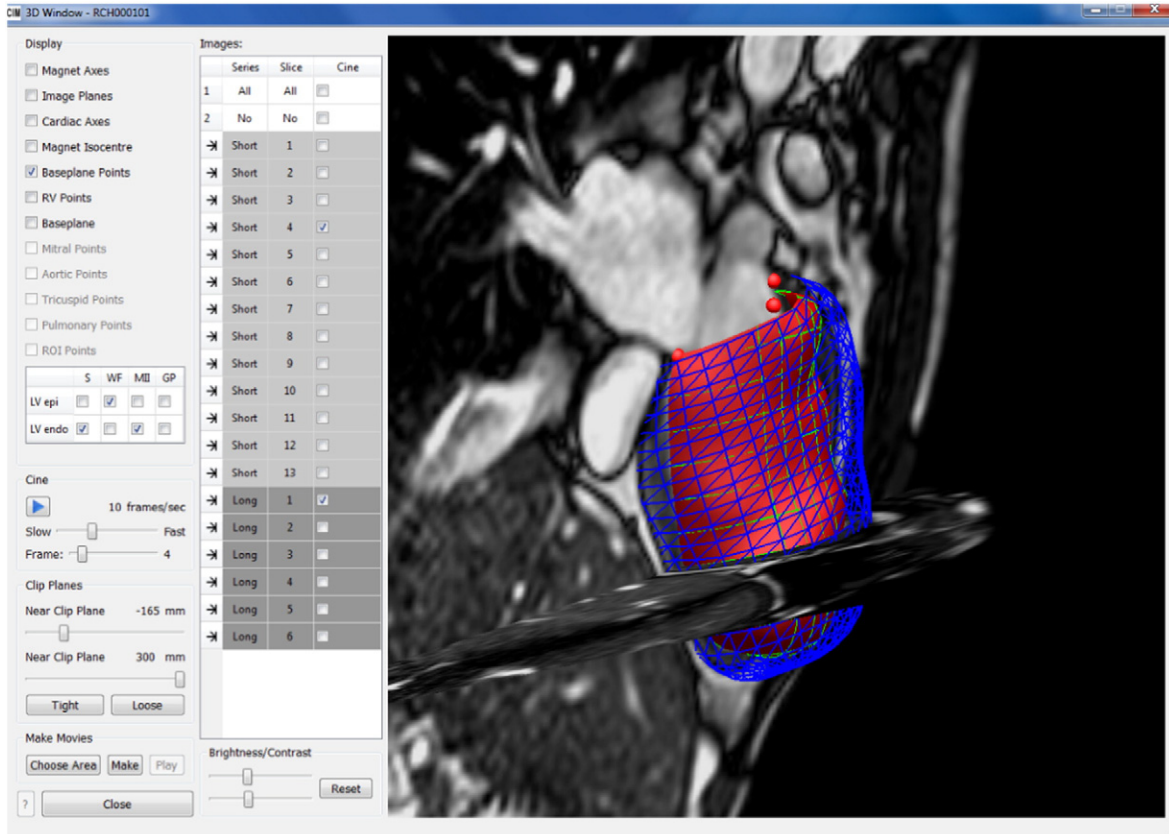


**Fig. 1.** Modeling tool for atlas-based ventricular shape modeling using cMRI.

[13–15,17–19]. In this study, the first five modes are used for all three PCA models. For  $PCA_{ED}$ , the percentages of shape variation explained by the first five modes were: 44%, 11%, 9%, 7%, 5%. Therefore, the first five modes explain 76% of the total variation in ED shapes in the asymptomatic population. For  $PCA_{ES}$ , the percentages of shape variation explained by the first five modes were: 43%, 11%, 7%, 5%, 4%. Therefore, the first five modes explain 71% of the total variation in ES shapes in the asymptomatic population. Furthermore, the first five modes have visually notable features and the purpose of this initial study was to assess shape and wall motion scores for the modes that could also be related to physician observations.

The previously reported [13] geometric manifestations of the first five statistical modes of shape variation in the population of asymptomatic controls are shown in Fig. 2 for the ED shape and in Fig. 3 for ES shape for reference. For each mode, the mean shape is juxtaposed with the  $+2\sigma$  and  $-2\sigma$  shape. Note that ED mode 1 is primarily dominated by variations in LV size, with the  $-2\sigma$  shape being significantly larger and the  $+2\sigma$  shape significantly smaller than the mean. The second and third modes appear to be dominated by differences in

sphericity and valve plane orientations. Mode four appears to capture variations in valve orientations. For the ES shapes, LV size also appears to dominate mode 1, and wall thickness variations appear to dominate mode 2. Mode 3 appears to be related to sphericity and valve orientation, and mode 4 captures variations associated with a combination of wall thickness and tilted valve orientation.

The first five modes of variation in the ventricular wall motions in the asymptomatic population [Fig. 4] are described in the results section. These modes represent different features of regional ventricular wall motions.

### 2.5. Calculation of CHD Patient-Specific Z-scores Relative to Control Population Data

To gain insight into shape abnormalities in CHD geometries at ED and ES, as well as functional abnormalities, Z-scores were calculated to describe how much an individual CHD patient differs from the control population mean. The following describes the calculation of the Z-scores for each CHD dataset for  $PCA_{ED}$ ,  $PCA_{ES}$  and  $PCA_{WM}$ .

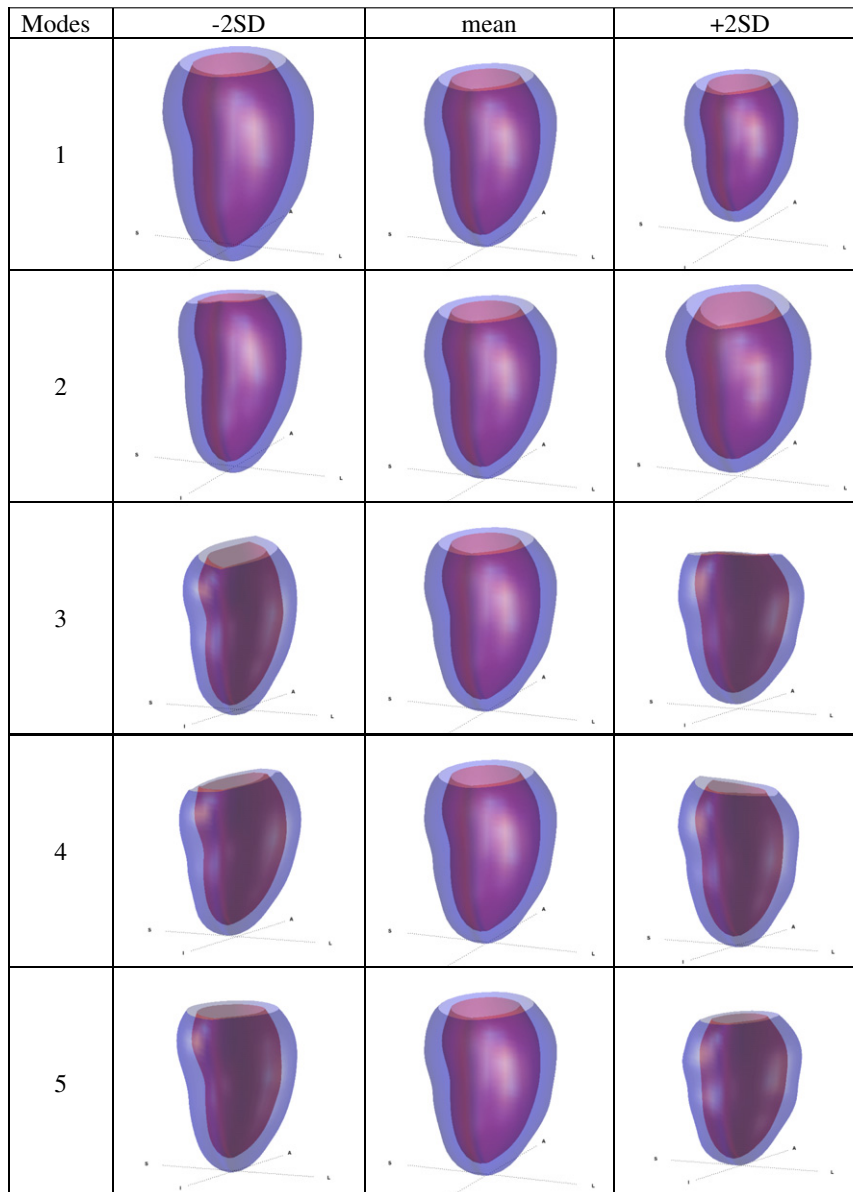


Fig. 2. The first five modes of asymptomatic shape variation at ED. Mean,  $-2SD$ , and  $+2SD$  shapes are shown to illustrate the geometric meaning of the modes.

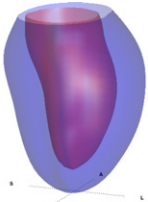
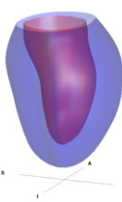
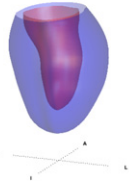
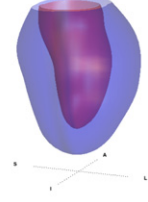
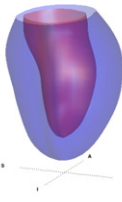
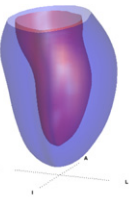
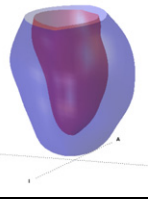
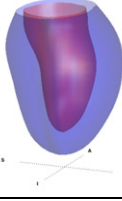
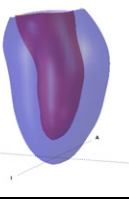
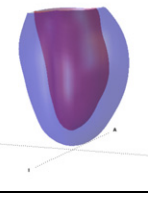
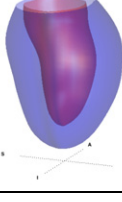
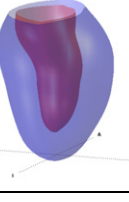
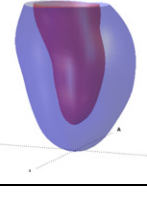
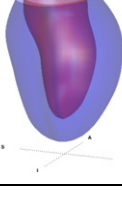
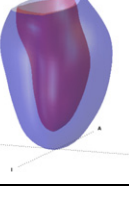
Modes	-2SD	mean	+2SD
1			
2			
3			
4			
5			

Fig. 3. The first five modes of asymptomatic shape variation at ES. Mean,  $-2SD$ , and  $+2SD$  shapes are shown to illustrate the geometric meaning of the modes.

Principal scores,  $b_s$ , were calculated for a patient shape,  $S$ , projected onto the PCA model,  $\Phi$ , of the control population, relative to the mean control shape,  $\bar{X}$ , as

$$b_s \Phi^{-1}(S - \bar{X})$$

Then, the Z-scores were calculated as follows. The standard deviation of the control principal score distribution for each mode  $j$  was calculated as

$$\sigma_j = \sqrt{\frac{1}{(N-1)} \sum_{i=1}^N \sum (b_{j,i} - \bar{b}_j)^2}$$

where  $b_{j,i}$  and  $\bar{b}_j$  are the principal scores and the mean of the  $j$ -th mode, respectively. Two times the standard deviation of the control principal score distribution was defined as the threshold signifying abnormal shape. The Z-scores for the CHD datasets are reported for the first five

mode of variation for  $PCA_{ED}$ ,  $PCA_{ES}$  and  $PCA_{WM}$ . Variations of each mode were then compared with the patient specific clinical data.

### 3. Results

#### 3.1. Analysis of ED and ES Shapes

##### 3.1.1. ED Shape Analysis

The ED shape analysis showed that all but one (Patient 1) of the CHD patients had at least one ED shape mode that was at least two standard deviations from the mean of the asymptomatic patients ( $Z > 2.0$ ) [Table 3]. For ED mode 1, none of the patients had a Z-score  $> 2$ , indicating that ventricular sizes in CHD patients were not significantly different from the normal group. For ED mode 2, four patients had Z-scores  $> 2$ , suggesting that abnormally increased sphericity may be a common feature of the CHD patient cohort. The highest Z-score ( $> 6$ ) occurred in ED mode 3 for patient 3. For ED modes 3, 4, and 5, three patients had Z-scores  $> 2$ . Each patient had elevated Z-scores in different modes, indicating that each patient has a ventricular shape with

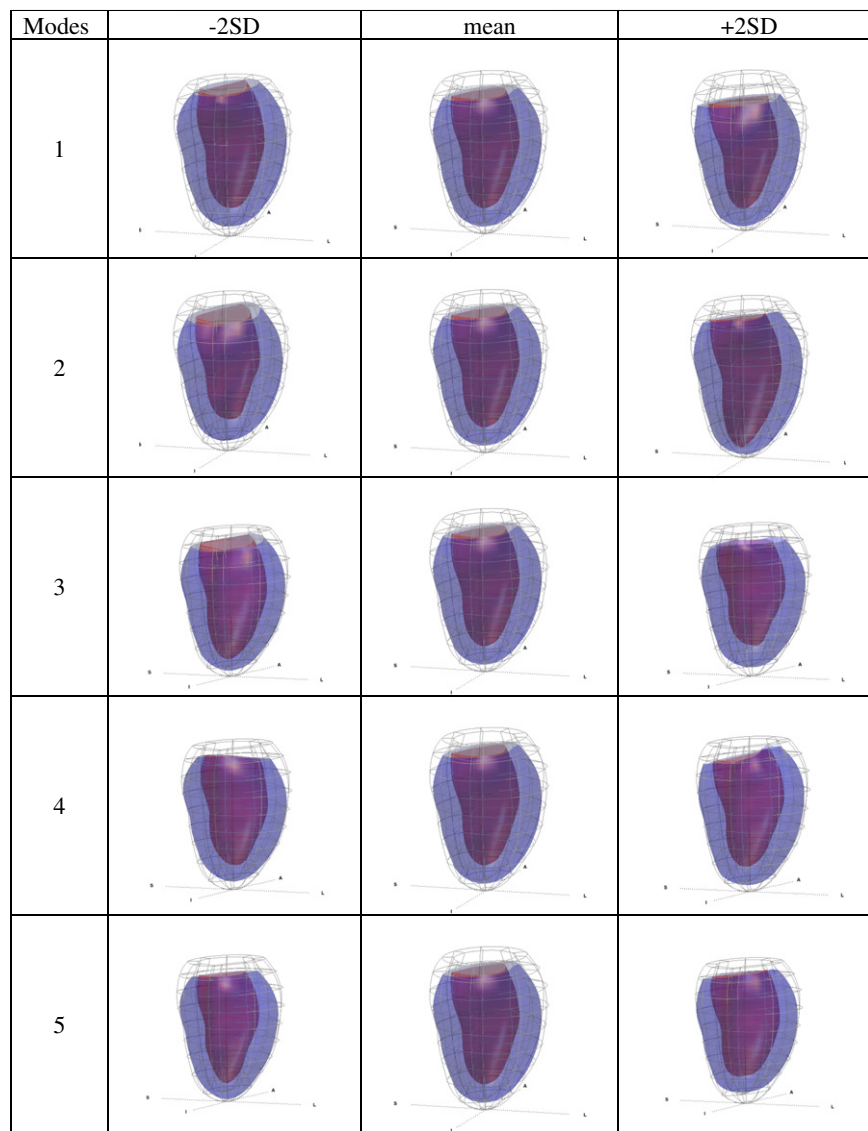


**Fig. 4.** The first five modes of variation in the wall motion between ED and ES. Mean,  $-2SD$ , and  $+2SD$  are shown to illustrate the physical meaning of the modes. Modes of variation in the displacement vectors are illustrated as an LV shape that describes the systolic deformation from the mean ED shape (shown as a gray wireframe).

measurable features that are different both from normal humans and from the other CHD patients.

### 3.1.2. ES Shape Analysis

The ES shape analysis showed that all but one (Patient 5) of the CHD patients had at least one ES Z-score that was at least two standard deviations from the mean of the asymptomatic hearts [Table 4], again indicating that the shape analysis method is quantifying characteristics of LV shape that are different from normal hearts. For ES mode 1, none of

the patients had a Z-score  $>2$ , again indicating that ventricular sizes in these adult CHD patients were not significantly different from normal. For ES mode 2, only patient 3 had an abnormal Z-score. For ES mode 3, five of the patients had Z-scores  $>2$ , indicating that abnormally increased end-systolic sphericity is also a feature common to a significant fraction of the CHD patient cohort. For ES mode 4, two patients had Z-scores  $>+2$ , indicating increased wall thickness, and two patients had scores  $<-2$ , indicating decreased wall thickness. Therefore abnormalities in end-systolic wall thickness features were present in

**Table 3**

End-diastolic shape analysis results: Z-score values of CHD patient shapes projected onto  $PCA_{ED}$ . Absolute values greater than  $2\sigma$  are highlighted in bold.

Patient	ED mode 1	ED mode 2	ED mode 3	ED mode 4	ED mode 5
1	-0.9	0.6	1.3	-1.5	-0.4
2	1.6	<b>3.1</b>	1.4	<b>-3.1</b>	<b>-2.0</b>
3	-0.7	1.6	<b>-6.6</b>	-1.6	-1.5
4	-0.7	<b>2.9</b>	-0.7	<b>-3.5</b>	-1.8
5	1.7	0.8	<b>2.3</b>	-0.6	-0.5
6	0.9	<b>4.5</b>	-0.7	<b>-2.8</b>	<b>-4.8</b>
7	1.3	<b>3.4</b>	-1.2	-1.8	-1.4
8	1.9	1.5	<b>3.4</b>	-0.7	<b>-2.3</b>

**Table 4**

End-systolic shape analysis results: Z-score values of CHD patient shapes projected onto  $PCA_{ES}$ . Absolute values greater than  $2\sigma$  are highlighted in bold.

Patient	ES mode 1	ES mode 2	ES mode 3	ES mode 4	ES mode 5
1	-1.3	-1.2	-0.2	<b>-3.4</b>	1.3
2	0.4	-1.8	<b>-2.7</b>	-1.3	1.2
3	-0.8	<b>3.3</b>	-0.8	<b>2.9</b>	<b>4.2</b>
5	-0.2	-1.8	<b>-3.0</b>	0.4	0.7
6	0.7	-1.2	-1.2	-1.0	0.8
7	0.2	1.4	<b>-2.1</b>	<b>2.0</b>	-1.9
8	1.4	<b>1.3</b>	<b>-2.0</b>	0.4	-0.5
9	1.0	-0.7	<b>-2.1</b>	<b>-2.8</b>	<b>-2.3</b>

half of the CHD cohort. For ES mode 5, two patients had Z-scores  $>2$  again indicating abnormal systolic wall thickness and valve orientation. Each patient had elevated Z-scores in different modes, indicating that each patient has a shape that is both different from normal and different from the other CHD patients.

### 3.1.3. Patient Specific Comparison of Shape Z-scores with Physician Observations

- Patient 1 had a Z-score of  $<-3\sigma$  in ES mode 4, which is associated with mitral valve orientation. This feature may be related to the restrictive valve motion observed in this patient. A low score in ES mode 4 is associated with decreased LV wall thickness. This might be consistent with the physician observation of mild dilation.
- Patient 2 showed  $>2\sigma$  values for ED modes 2 and 4, and ES mode 3. All three of these modes are associated with altered valve orientation. The negative value in ES mode 4 and the positive value in ED mode 2 are indicative of increased sphericity.
- Patient 3 has an unusual LV shape, which is elongated and slightly curved around the RV apex. A large negative value in ED mode 3, indicative of decreased sphericity, makes sense given the elongated shape.
- Patient 4 had physician observations of mild mitral and aortic regurgitation and a dilated aortic root. This patient had a low Z-score in ED mode 4 and ES mode 3, which are indicative of altered valve orientation and may reflect effects of the altered anatomy observed at the base of the LV. The clinical observations also included moderate LV dilation. This patient had high ED mode 2 and low ES mode 3, which are indicative of an abnormally spherical LV shape.
- Patient 5 had a score of  $>2\sigma$  in ED mode 3, which is associated with increased sphericity and abnormal valve orientation.
- Patient 6 had a high score  $>4\sigma$  in ED mode 2, indicative of increased sphericity, low  $>2\sigma$  ED mode 4 indicative of altered valve orientation, and low  $>2\sigma$  ES mode 3 indicating increased sphericity and 4 decreased wall thickness. However, this patient had no observed dilation and normal systolic function.
- Patient 7 had high  $>3\sigma$  ED mode 2, indicative of increased sphericity, and low  $>2\sigma$  ES mode 2 indicating increased wall thickness and ES mode 3 indicating increased sphericity. This patient had no hypertrophy or dilation and normal systolic function.
- Patient 8 had a high score ( $>3$ ) in ED mode 3, and a low score ( $<-2$ ) in ES mode 3, both indicating increased sphericity. A low score ( $Z < -2$ ) in ES mode 4 suggested decreased wall thickness and altered valve orientation. This patient had no observation of dilation and had normal systolic function.

## 3.2. Analysis of Wall Motions

### 3.2.1. Modes of Variation in Wall Motion for the Asymptomatic Population

Geometric renderings of the first five systolic wall motion modes ( $PCA_{WM}$ ) for the asymptomatic population are shown superimposed on the mean ED shape in Fig. 4. Mode 1 is dominated by longitudinal shortening, including vertical base-plane movement. Mode 2 is also associated with longitudinal movement, but more prominently at the apex, and includes variations in apical wall thickening. Mode 3 captures variations in base plane displacements in the inferior-posterior plane and some systolic wall thickening. Mode 4 is mainly associated with base plane movement in the lateral-septal plane. Mode 5 describes overall contraction of the ventricle. The percentages of variation in  $PCA_{WM}$  explained by the first five modes were: 21%, 13%, 10%, 8%, 6%. Therefore, the first five modes explain 58% of the total variation in ventricular wall motion in the asymptomatic population.

### 3.2.2. CHD Wall Motion Z-scores

All CHD patients had at least one Z-score over 2 in magnitude, indicating that ventricular wall motions were significantly different from normal in some major respect [Table 5]. None of the patients had Z-scores  $>2$  in Mode 1, but four patients had Z-scores  $>2$  in Mode 2. Two patients had scores  $>2$  in Mode 3, and three patients had scores  $>2$  in Mode 4.

Mode 5 showed the highest Z-scores, with all eight CHD patients exceeding two standard deviations from the mean of normal hearts. Mode 5 was associated with global LV contraction. The high Z-scores in mode 5 indicate that the CHD ventricles showed significantly less LV contraction than normal hearts. Thus this score can be compared with global ejection fraction as a measure of ventricular function. Patients 3, 4, and 7 had low-normal systolic function ( $EF = 55\%$ ). Patients 3 and 4 had a mode 5 Z-score  $>4$ , and patient 7 had a Z-score  $>3$ . For these patients, the high Z-scores were a more sensitive index of ventricular dysfunction than EF. The patient with the lowest EF (Patient 1,  $EF = 52\%$ ) did have an elevated Z-score ( $>3$ ), but did not have the greatest score. In apparent contrast, patient 9 had a mode 5 Z-score  $>3$ , but had a normal EF of 59%. Thus, there was no strong correlation between EF and wall motion mode 5 ( $R^2 = 0.2$ ); rather, the wall motion Z-scores quantified more specific wall motion abnormalities.

## 3.3. Potential Relationships Between Shape and Wall Motion

In the cohort of eight tricuspid atresia patients, correlations between shape Z-scores and wall motion Z-scores revealed two interesting observations. The first was a correlation ( $R^2 = 0.63$ ) between wall motion mode 1 and ED mode 3. Wall motion mode 1 is associated with longitudinal shortening during systole, and ED mode 3 is associated with LV sphericity. Therefore, an ED shape that was more spherical tended to coincide with a functional difference in which the longitudinal shortening during systole was reduced.

The second finding was a correlation ( $R^2 = 0.52$ ) between wall motion mode 5 and ED mode 1. Wall motion mode 5 is associated with overall LV contraction, and ED mode 1 is associated with LV size. Therefore, an ED shape that was larger in size tended to coincide with decreased ventricular contraction during systole.

## 4. Discussion

The ED and ES shape analyses showed consistent results. In both separate analyses, the mode associated with LV size was found to *not* show abnormality exceeding the threshold value. Additionally, both analyses separately showed that sphericity is abnormally increased in at least half of the CHD patient cohort. The similarity in results between the ES and ED analyses suggests that the method is indeed consistently capturing the aspects of altered LV shape relevant in the CHD patients.

Plausible relationships between physician observations and quantitative shape statistics were found in four patients, and relationships between visually apparent features of ventricular morphology and shape statistics and were seen in six patients. Thus these quantitative shape statistics derived from principal components of normal ventricular

**Table 5**

Wall motion analysis results: Z-score values of CHD patient shapes projected onto  $PCA_{WM}$ . Absolute values greater than  $2\sigma$  are highlighted in bold.

Patient	Disp mode 1	Disp mode 2	Disp mode 3	Disp mode 4	Disp mode 5
1	-1.1	1.4	-1.7	<b>-2.4</b>	<b>3.1</b>
2	-1.4	<b>2.5</b>	<b>-2.2</b>	-1.7	<b>2.8</b>
3	0.5	1.8	-0.4	<b>-2.2</b>	<b>4.3</b>
5	-0.4	-0.1	0.4	-1.1	<b>4.8</b>
6	-0.9	<b>2.3</b>	<b>-2.6</b>	-1.1	<b>2.5</b>
7	-0.4	<b>3.1</b>	-1.8	-1.5	<b>2.8</b>
8	-0.5	1.2	-0.2	-1.7	<b>3.3</b>
9	-0.5	<b>2.1</b>	<b>-2.1</b>	-1.1	<b>3.2</b>

anatomy appear to be capable of quantifying abnormal features of ventricular geometry present in single ventricle CHD patients.

For the wall motion modes,  $PCA_{WM}$ , which quantify the statistical modes of variation in the myocardial deformation of the asymptomatic hearts between ED and ES, the total variation explained by the first five modes was less (58%) than that of the shape variations (76% for  $PCA_{ED}$  and 71% for  $PCA_{ES}$ ). In future studies with larger cohorts it may be useful to consider a greater number of modes to more fully capture variations in systolic deformation.

The analysis of systolic deformations showed that all CHD patients had some abnormal LV contractile function as expected, even though many of the patients had ejection fractions in the normal range. There did not appear to be any strong correlations between EF and the wall motion statistics; hence, this analysis may be quantifying novel aspects of altered wall motion that are not detected by global volumetric measurements.

The correlation between a more spherical ED shape and decreased longitudinal shortening in the deformation is consistent with previous studies of acquired heart failure and dyssynchrony [18]. More spherical LV shape has been reported during the progression to HF in animals and humans [4,6], and decreased systolic ventricular shortening is a well-known characteristic of the failing heart [18]. The quantitative correlation of these two characteristics in the CHD group suggests there may be a mechanistic link or that changes in ventricular sphericity and wall motion mode 5 might be early markers of systolic dysfunction in single ventricle physiology.

The second correlation, between LV size at ED and contractile function is also noteworthy. This correlation suggests a relationship between dilation and decreased systolic function in CHD that may be causal. Indeed, the patient with the lowest EF also showed mild dilation by clinical observation. Most patients with single ventricle physiology also have some component of valvular insufficiency that imposes a volume load and ventricular stretch. These are commonly associated with right and left HF conditions in CHD [7,19].

The shape analysis approach employed here was able to identify two key correlations between shape and function, both of which are broadly consistent with expectations about the progression of ventricular remodeling to contractile dysfunction and heart failure. These correlations themselves do not imply causality, but the quantitative three-dimensional models developed for the shape analysis are also suitable to develop patient-specific models of ventricular mechanics that could test for a mechanistic relationship. Thus, the methods employed in this study appear to have potential for uncovering more detailed relationships between shape and function. These relationships could be used to define shape parameters as early markers of disease, and could better inform the assessment of patient risk.

#### 4.1. Limitations

Age-matched asymptomatic population data was not available for use in this study. The age range of the asymptomatic population was 45–85, whereas the age range of the CHD patients in this study was 13–45. The CAP database is currently being expanded to include more MR imaging data from a wider age range of both CHD patients and asymptomatic volunteers. This will enable future studies to compare CHD patient geometries with age and gender matched sub-cohorts. Secondly, the number of CHD patients analyzed in this study was relatively limited. Eight patients were sufficient to achieve the goal of evaluating the basic utility of the shape analysis approach and developing new hypotheses. However, this is not large enough for assessing trends in shape and wall motion characteristics in CHD.

## 5. Conclusions

The first application of atlas-based shape analysis to single ventricle congenital heart disease reported here shows promise for quantifying

alterations in ventricular geometry that are specific to congenital heart disease and may be candidate indicators of adverse ventricular remodeling. In particular, abnormalities in modes of shape variation associated with ventricular sphericity, ventricular wall thickness, and base plane orientation were quantified for the CHD patients. Atlas-based shape analysis also showed promising results for characterizing alterations in ventricular wall motion relevant in CHD, as a potentially more detailed measure of LV function. The wall motion analysis quantified aspects of altered systolic function which may not be detectable with global volume measures such as ejection fraction. Lastly, we showed that atlas-based shape analysis can identify quantitative relationships between shape and systolic wall motion. In particular, this study pointed toward potential relationships between increased sphericity in ED shape and decreased longitudinal shortening in the deformation, and between increased LV size and decreased LV function that should be tested in larger patient cohorts.

A unique feature of single-ventricle CHD patients is that repeated MR imaging is common in the clinical setting, spanning years of cardiac remodeling. Longitudinal studies of the progression of ventricular remodeling using atlas-based shape modeling could lead to more insight into early detection of maladaptive characteristics.

This study pointed toward relationships between LV size (which could be related to dilation) and function, and between sphericity and decreased longitudinal shortening. These relationships are likely related to the physical mechanics of ventricular deformation. Finite element models of ventricular wall mechanics can be used to test the mechanical basis of relationships between shape and systolic function identified with the techniques described here and will reveal new information about mechanical stress distributions in the single ventricle heart, which are thought to play a role in adverse remodeling. Biomechanical parameters could also be correlated with measures of altered shape in order to discover early markers of patient risk.

Atlas-based shape analysis shows promise for quantifying important aspects of ventricular shape in CHD, tracking more detailed patient data over time, and may eventually lead to improved understanding of patient risk. The relative speed of creating these models compared with more conventional segmentation methods makes it feasible for clinical application, and for creating larger CHD databases in the CAP.

## Competing Interests

ADM is a co-founder of and has an equity interest in Insilicomed, Inc., and he serves on the scientific advisory board. Some of his research grants, including those acknowledged here, have been identified for conflict of interest management based on the overall scope of the project and its potential benefit to Insilicomed, Inc. The author is required to disclose this relationship in publications acknowledging the grant support, however the research subject and findings reported here did not involve the company in any way and have no relationship whatsoever to the business activities or scientific interests of the company. The terms of this arrangement have been reviewed and approved by the University of California San Diego in accordance with its conflict of interest policies. The other authors have no competing interests to declare.

## References

- [1] Alfakih K, Plein S, Thiele H, Jones T, Ridgway JP, Sivanathan MU. Normal human left and right ventricular dimensions for MRI as assessed by turbo gradient echo and steady-state free precession imaging sequences. *J Magn Reson Imaging* 2003;17:323–9.
- [2] Brickner ME, Hillis LD, Lange RA. Congenital heart disease in adults - (second of two parts). *N Engl J Med* 2000;342:334–42.
- [3] Brickner ME, Hillis LD, Lange RA. Congenital heart disease in adults: First of two parts. *N Engl J Med* 2000;342:256–63.
- [4] Cohn JN. Critical review of heart failure: the role of left ventricular remodeling in the therapeutic response. *Clin Cardiol* 1995;18:IV4–12.
- [5] Fonseca CG, Backhaus M, Bluemke DA, Britten RD, Chung JD, Cowan BR, Dinov ID, Finn JP, Hunter PJ, Kadish AH, Lee DC, Lima JA, Medrano-Gracia P, Shivkumar K,



- Suinesiaputra A, Tao W, Young AA. The cardiac atlas project—an imaging database for computational modeling and statistical atlases of the heart. *Bioinformatics* 2011;27:2288–95.
- [6] Francis GS. Changing the remodeling process in heart failure: basic mechanisms and laboratory results. *Curr Opin Cardiol* 1998;13:156–61.
- [7] Khairy P, Van Hare GF, Balaji S, Berul CI, Cecchin F, Cohen MI, Daniels CJ, Deal BJ, Dearani JA, Groot N, Dubin AM, Harris L, Janousek J, Kanter RJ, Karpawich PP, Perry JC, Seslar SP, Shah MJ, Silka MJ, Triedman JK, Walsh EP, Warnes CA. PACES/HRS expert consensus statement on the recognition and management of arrhythmias in adult congenital heart disease: developed in partnership between the pediatric and congenital electrophysiology society (PACES) and the Heart Rhythm Society (HRS). Endorsed by the governing bodies of PACES, HRS, the American College of Cardiology (ACC), the American Heart Association (AHA), the European Heart Rhythm Association (EHRA), the Canadian Heart Rhythm Society (CHRS), and the International Society for Adult Congenital Heart Disease (ISACHD). *Heart Rhythm* 2014;11:e102–65.
- [8] Leary PJ, Kurtz CE, Hough CL, Waiss MP, Ralph DD, Sheehan FH. Three-dimensional analysis of right ventricular shape and function in pulmonary hypertension. *Pulm Circ* 2012;2:34–40.
- [9] Leonardi B, Taylor AM, Mansi T, Voigt I, Sermesant M, Pennec X, Ayache N, Boudjemline Y, Pongiglione G. Computational modelling of the right ventricle in repaired tetralogy of Fallot: can it provide insight into patient treatment? *Eur Heart J Cardiovasc Imaging* 2013;14:381–6.
- [10] Lewandowski AJ, D. Augustine, P. Lamata, E. F. Davis, M. Lazdam, J. Francis, K. McCormick, A. R. Wilkinson, A. Singhal, A. Lucas, N. P. Smith, S. Neubauer and P. Leeson. Preterm heart in adult life cardiovascular magnetic resonance reveals distinct differences in left ventricular mass, geometry, and function. *Circulation* 127: 197–+, 2013.
- [11] Marelli AJ, Mackie AS, Ionescu-Ittu R, Rahme E, Pilote L. Congenital heart disease in the general population - changing prevalence and age distribution. *Circulation* 2007;115:163–72.
- [12] Medrano-Gracia P, Backhaus M, Bluemke DA, Do Chung J, Cowan BR, Finn JP, Fonseca CG, Hunter PJ, Kadish AH, Lee DC. The cardiac atlas project: rationale, design and preliminary results. *J Cardiovasc Magn Reson* 2011;13:1–2.
- [13] Medrano-Gracia P, Cowan BR, Ambale-Venkatesh B, Bluemke DA, Eng J, Finn JP, Fonseca CG, Lima JAC, Suinesiaputra A, Young AA. Left ventricular shape variation in asymptomatic populations: the multi-ethnic study of atherosclerosis. *J Cardiovasc Magn Reson* 2014;16.
- [14] Medrano-Gracia P, Cowan BR, Finn JP, Fonseca CG, Kadish AH, Lee DC, Tao WC, Young AA. The cardiac atlas project: preliminary description of heart shape in patients with myocardial infarction. *Stat Atlases Comput Model Heart* 2010;6364:46–53.
- [15] Piran S, Veldtman G, Siu S, Webb GD, Liu PP. Heart failure and ventricular dysfunction in patients with single or systemic right ventricles. *Circulation* 2002;105:1189–94.
- [16] Remme EW, Young AA, Augenstein KF, Cowan B, Hunter PJ. Extraction and quantification of left ventricular deformation modes. *IEEE Trans Biomed Eng* 2004;51:1923–31.
- [17] Sluysmans T, Sanders SP, Vandervelde M, Matitiau A, Parness IA, Spevak PJ, Mayer JE, Colan SD. Natural-history and patterns of recovery of contractile function in single left-ventricle after Fontan operation. *Circulation* 1992;86:1753–61.
- [18] Tejman-Yarden S, Bratincsak A, Bachner-Hinenzon N, Khamis H, Rzasa C, Adam D, Printz BF, Perry JC. Left ventricular mechanical property changes during acute AV synchronous right ventricular pacing in children. *Pediatr Cardiol* 2016;37:106–11.
- [19] Warnes CA, Williams RG, Bashore TM, Child JS, Connolly HM, Dearani JA, del Nido P, Fasules JW, Graham Jr TP, Hijazi ZM, Hunt SA, King ME, Landzberg MJ, Miner PD, Radford MJ, Walsh EP, G. D. Webb. ACC/AHA. Guidelines for the management of adults with congenital heart disease: a report of the American College of Cardiology/American Heart Association Task Force on Practice Guidelines (writing committee to develop guidelines on the management of adults with congenital heart disease). *Circulation* 2008;118(e714–833):2008.
- [20] Young AA, Cowan BR, Thrupp SF, Hedley WJ, Dell'Italia LJ. Left ventricular mass and volume: fast calculation with guide-point modeling on MR images. *Radiology* 2000;216:597–602.
- [21] Zhang XY, Cowan BR, Bluemke DA, Finn JP, Fonseca CG, Kadish AH, Lee DC, Lima JAC, Suinesiaputra A, Young AA, Medrano-Gracia P. Atlas-based quantification of cardiac remodeling due to myocardial infarction. *Plos One* 2014;9.